

# **Effect of Reactive Elements on Porosity in Spray-Formed Copper-Alloy Billets**

**Hilmar R. Müller, Klaus Ohla, Robert Zauter, Michael Ebner**

Wieland-Werke AG

Graf-Arco-Strasse 36, D-89079 Ulm

e-mail: [Hilmar.Mueller@Wieland.de](mailto:Hilmar.Mueller@Wieland.de)

phone: +49-731-944-3697

fax:+49-731-944-4729

## **Abstract**

In spray formed preforms, porosity is unavoidable. The atomising gas is entrapped during the process. Normally nitrogen is used and therefore the voids are filled with this gas. Unfortunately, nitrogen is not soluble in copper. To obtain a dense material after further forming processes such as extrusion, forging or drawing, porosity has to be limited to a specified level.

There are means to influence porosity inside the spray-formed billet. Up to a certain extent porosity can be influenced by process parameters such as melt temperature, metal mass flow and/or Gas-/Metal flow-rate ratio (G/M). Reactive elements inside the alloy (e.g. Ti) have an additional effect. This phenomenon is reported previously [2],[9],[10]. It is explained by reaction of reactive elements such as Zr, Ti, Al et. al. with the

entrapped nitrogen. But a detailed quantitative explanation has not been pointed out. A theory of hot porosity formation is presented. The calculation and analytical methods are described. The theoretical and experimental results are discussed.

Keywords: Spray forming, porosity, copper alloys, reactive elements

## **Introduction**

Quality issues require limitation of as-sprayed porosity for subsequent processing of spray-formed copper-alloy billets to a certain level. This porosity can only be minimised when the parameters influencing porosity are identified. These are described previously by various authors. Pores can be formed inside the droplets by gas entrapment during droplet formation, dissolution of gas from molten metal, solidification shrinkage or collision between larger liquid and smaller solidified droplets [1].

During deposition the fraction of solid  $f_s$  is most important. At a high fraction of solid  $f_s$  the pores arise from poor spreading of droplets and insufficient liquid feeding [1].

Interstices between adjacent droplets arriving at the surface leave irregular cavities [2]. This effect can be intensified by a high heat extracting substrate. The layers near the substrate are more porous than the bulk material [2],[3],[4].

At a low fraction of solid  $f_s$  the interstices between solid particles can be fed by liquid metal and porosity decreases. Apparently there are some contrary results. For example Akhlaghi [1], Doherty [5] and Warner [3] describe that a low liquid fraction  $f_l$  results in high percentages of pre-solidified droplets and porosity. On the contrary, Chu [6] reports that bulk porosity increases as fraction of liquid  $f_l$  in the spray cone increases

when impacting on mushy surface. It is explained by the state of the mushy layer on the top of the deposit. At a high fraction of liquid  $f_l$  the mushy layer is thick and hot. Therefore, viscosity is low. The mushy layer is continuously disturbed by the high velocity gas jet and atomised droplets. When the droplets hit the mushy surface, they entrain the surrounding gas [7]. It is therefore expected that  $f_l$  has an upper and a lower limit for preventing either gas porosity or cold porosity.

Another type of porosity is caused by the so-called cauliflower-effect. It occurs during spray deposition in the centre of the billet when many solidified droplets are collected [8] .

The minimising effect on porosity by reactive elements is reported by Watson [9], [2] and Cooney [10] . The latter recommends strong nitride formers such as silicon and chromium. Watson named as preferred elements aluminium, silicon, titanium, chromium and zirconium. The formation of nitrides changes the surface tension of the droplets. This influences the behaviour of the droplets during the impact of the mushy layer and therefore the entrainment of gas [7] . All the reported types of porosity can be classified into two classes: cold and hot porosity (Fig. 1).

## **Porosity in copper billets**

### **Definition and measurement of porosity**

Porosity is defined by the following equation:

$$Pt = \left(1 - \frac{\bar{\rho}}{\rho_0}\right) * 100 \quad (1)$$

$Pt$  : Porosity in %

$\rho_0$  : Mass density of material without pores. Not the theoretical but the measured density of hot and cold worked material is used.

$\bar{\rho}$  : Mass density as measured in the deposit

The density is measured with a buoyancy weighing-machine according to DIN EN 6018. The specimens are 10 x 10 x 10 mm<sup>3</sup> cubes [11] . The results are compared with pictures of the microstructure at 50 x magnification. **Fig. 2, Fig. 3 and Fig. 4** give an impression of the measured data for 3 different alloy types. Especially samples with low porosity could show poorer consistency between photograph and measured figures. Measurement by buoyancy takes the whole sample volume into account. In the case of the photograph, only the surface is evaluated. Some isolated pores inside the sample can influence the measured result but they are not visible on the surface.

### **Process parameters influencing porosity**

The most important parameter is the Gas-to-Metal flow-rate ratio G/M as reported elsewhere [12] . It is not only important for porosity but for segregation too. In production plants the minimum G/M ratio is not limited by an increasing porosity caused by the lower viscosity of the mushy layer and therefore an increased gas

entrainment (see Introduction, [6] ). The limiting factor is damage to the billet by centrifugal forces. Large pieces of partly solidified material are expelled.

Further parameters are metal flow rate, melt temperature, flying distance of the droplets, gas and droplet velocity, spray cone angle and scanning angle. But these parameter are not discussed in this paper. The focus is on the effect of reactive elements.

### **Reactive elements influencing porosity**

We think that the entrainment of gas by the droplets hitting the liquid surface of the deposit is the main reason for hot porosity. This effect is boosted by cavities in the solidified droplets. Partly solidified droplets collide with rigid particles. Some of them are embedded, others break out and leave cavities. In **Fig. 5** at position **a**, a droplet is embedded and completely welded. At position **b**, a particle broke out and left a crater. It cannot be identified if this happened during flight or after preparation of the sample. At position **c**, the particle which formed the crater lost contact before collision with particle **a**. Crater **c** is deformed by this collision. Such craters increase gas entrainment when the droplets dive into the liquid layer on the deposit.

The elements zirconium and titanium were tested in preliminary trials. Their effect on porosity is evaluated as equivalent. So for the following tests only titanium was added to the melt during normal production of numerous billets. One slice was cut from each end and density was measured at three radial positions (edge, median, centre). This was carried out on three different alloy groups represented by  $\text{CuAl13Fe4.5CoMn}$ ,  $\text{CuSn13.5}$  and  $\text{CuMn20Ni20}$ . All results are collected in data files, the average and standard deviation is computed and plotted in diagrams (**Fig. 6**, **Fig. 7** and **Fig. 8**).

The addition of 0.25 wt% Pb to CuAl13Fe4.5CoMn increases density significantly. It is not a reactive element, but it increases fluidity of the mushy zone due to the low melting point. As a result, the interstices between solidified particles are filled. The higher density of lead in comparison with copper is negligible because of the low content. A further increase in density is observed after adding 0.15 wt% titanium to the melt.

The alloy CuSn13.5Pb contains about 0.5 wt% lead. The addition of 0.15 wt% titanium in the melting furnace reduces porosity as described for CuAl13Fe4.5CoMn (Fig. 7). A similar result is shown by Fig. 8 for the alloy CuMn20Ni20.

The effect of reactive elements on porosity due to the formation of nitrides is reported in the introduction. In the following this theory is proved by measurement and calculation.

### **Analysis of nitrides**

The method described by Hedges [13] was adapted to CuSn. Samples for phase extraction were accurately machined cylinders 50 mm x 6 mm in diameter. Each cylinder was cleaned using 400  $\mu\text{m}$  SiC paper before extraction. Secondary phases were extracted electrolytically at a current density of 3 mA/mm<sup>2</sup> in a solution of 10 % HCl in methanol. The sample, which acted as the anode, was suspended in the acid solution such that it was submerged 30 mm below the liquid level and concentrically located in a shaped stainless steel sheet that was used as the cathode (Fig. 9). The CuSn matrix was gradually dissolved and the secondary phases settled to the bottom of the beaker. The electrolyte was then filtered, as shown in Fig. 10, and the secondary phase particles were collected on a glass micro fibre paper using a filter connected to a vacuum pump.

To give crystallographic information, an analysis was performed on the extracted phases with the X-ray diffractometer STADI P (STOE & CIE GmbH, Darmstadt). The X-ray diffraction diagram (**Fig. 11**) shows the result. There is a striking evidence for TiN in the extract. This is confirmed by X-ray diffraction on the undissolved spray formed sample with the ARL diffractometer X`TRA [14] .

### **The effect of titanium on porosity**

The following assumptions are made for a calculation of the entrained nitrogen and reaction with titanium:

- The entrained gas bubbles adapt their temperature to the surrounding metal immediately.
- Solidification time of the mushy layer allows the reaction of titanium and nitrogen. Watson [9] indicating 5 to 22 seconds for a strip and Doherty [5] 10 to 200 seconds for a billet. Compared with this, the reaction time during flight is only a split-second (droplet speed 50 - 100 m/s, flight distance 600 mm).
- During solidification, the bubble pressure is constant. Because of the relative thin liquid layer the metalostatic pressure is neglected. The initial pressure in the bubble is equal to the spray chamber pressure.
- The bubble volume changes isobarically until solidus temperature is reached. When they are enclosed in regions of higher solid fraction  $f_s$ , they are fed with liquid metal through channels with low melting phases (**Fig. 12**). With further cooling, the bubble (pore) volume changes only by shrinkage of the surrounding metal.
- The pores are regularly (like a ball) or irregularly shaped.

- The gas in the bubble behaves ideally.

The overall volume  $V_P$  of the pores in a deposit of the mass  $m_D$  can be calculated from the measured density, using the definition of porosity in equation (1).

$$V_D = m_D / \bar{\rho} \quad (2)$$

$$V_P = Pt * V_D \quad (3)$$

$V_D$  : volume of the deposit

$m_D$  : mass of the deposit

$V_P$  : volume of all pores in the deposit

Therefore, density of the gas is kept constant during cooling to solidus temperature, density at ambient temperature can be calculated taking into consideration the shrinkage of the surrounding metal during cooling from solidus to ambient temperature:

$$\rho_a = \rho_{sol} (1 + 3\alpha(T_{sol} - T_E)) \quad (4)$$

$\rho_a$  : density of gas at ambient temperature

$\rho_{sol}$  : density at solidus temperature

$T_{sol}$  : absolute solidus temperature

$\alpha$  : linear thermal expansion coefficient

The cooling from solidus to ambient temperature decreases the pressure in the bubbles. This effect is counteracted by the shrinkage of the surrounding metal. According to the law of ideal gas the pressure is:

$$P_a = P_{sol} \frac{\rho_a T_a}{\rho_{sol} T_{sol}} \quad (5)$$

$P_a$  : pressure in the pores at ambient temperature

$T_a$  : absolute ambient temperature

The number of moles  $N_2$  in the deposit is now defined:

$$n = \frac{P_d V_P}{RT_a} \quad (6)$$

$n$  : number of moles  $N_2$

$R$  : molar gas constant

The mass and concentration of  $N_2$  in the deposit can now be calculated using the molar mass of N:

$$m_{N_2} = 2nM_N \quad (7)$$

$$c_{N_2} = \frac{m_{N_2}}{m_D} \quad (8)$$

$m_{N_2}$  : mass of nitrogen in the deposit

$M_N$  : molar mass of nitrogen

$c_{N_2}$  : concentration of nitrogen in the deposit

The concentration was measured by hot extraction with the LECO ON-Analysator TC 600 [15]. In Table 1, the measured concentrations  $c_{N_2,m}$  (grey shaded column) are compared with the calculated concentration  $c_{N_2,min}$  and  $c_{N_2,max}$ .

As the samples for density measurement and nitrogen analysis are from the same billet but not identical, the nitrogen concentration is calculated with the minimum and maximum density measured in the billet. The measured nitrogen concentration  $c_{N_2,m}$  is nearly as high as the calculated maximum  $c_{N_2,max}$ . This confirms the theory that in copper-base alloys without reactive elements the nitrogen is entrapped in the pores.

The reaction of titanium with nitrogen can be proved by a similar calculation. Using Equation (3) the pore volume is calculated by inserting in the measured density with and without titanium. The volume difference is the amount of nitrogen, which reacted with titanium to TiN.

$$\Delta V_P = V_P - V_{P,Ti} \quad (9)$$

$$m_{Ti} = 2nM_{Ti} \quad (10)$$

$$c_{Ti} = \frac{m_{Ti}}{m_D} \quad (11)$$

$\Delta V_P$  : pore volume difference between deposits with and without titanium

$V_P$  : pore volume without titanium

$V_{P,Ti}$  : pore volume with titanium

$m_{Ti}$  : mass of titanium in the deposit

$c_{Ti}$  : concentration of titanium, which is necessary for reducing the porosity from Pt to PtTi

The mass and the concentration of TiN are:

$$m_{TiN} = 2n(M_{Ti} + M_N) \quad (12)$$

$$c_{TiN} = \frac{m_{TiN}}{m_D} \quad (13)$$

$m_{TiN}$  : mass of TiN in the deposit

$c_{TiN}$  : concentration of TiN in the deposit

**Table 1** shows an example calculation for CuMn20Ni20. The grey coloured fields are input data. The measured densities are from **Fig. 8**. The difference in density with and

without Ti seems to be very small but in terms of porosity there is a factor of 3. The minimum concentration of Ti in the melt for this reduction of porosity is very low. The presence of TiN is proved (Fig. 11).

The quantitative analysis of the TiN concentration in CuMn20Ni20Ti was performed with the experimental set up shown in Fig. 9 and Fig. 10. The CuMn20Ni20 sample was dissolved with 0.6 A initial current. After 1 h the current was increased to 1 A and after another 2 hours to 1.2 A. After 5.5 h total time the submerged part of the sample was dissolved. Then the electrolyte was filtered and washed with diluted nitric acid (30 %). After reaction with potassium peroxydisulfate the remainder was dissolved in a heated Pt-crucible with sulphuric acid and analysed by Inductively Coupled Plasma atomic emission spectrometry (ICP). The concentration of TiN in the sample determined by this method was 0.0008 %. Compared with the calculated value Table 1 the measured figure is 4 times higher than the calculated one but of the same order of magnitude. The calculated figure is based on statistical average values. The measured figure is based on a single sample. Therefore a perfect match cannot be expected.

The probability of formation of TiN is estimated by an equilibrium calculation with the Outokumpu-Software HSC [16]. The main input parameters and results are given in Fig. 13. The atomized alloy is CuMn20Ni20 with 0.15 wt% Ti addition. The atomising gas is nitrogen with a little amount of oxygen impurities. Unfortunately, the kinetics cannot be calculated. But the equilibrium calculation shows, that, at melt temperature of the atomisation process of about 1100 °C, the TiN dominates. At lower temperatures, the equilibrium changes to Mn-nitrides and Mn-oxide. At these temperatures the

solidification process is finished and the reaction velocity is reduced, so that the Mn-nitride formation is negligible.

## **Conclusion**

Porosity in spray-formed copper-base alloys is classified into two classes: cold and hot porosity. It is influenced by process parameters and by the addition of reactive elements, e.g. Ti. The most important process parameter is the Gas-/Metal flow rate ratio G/M. Calculations and measurements show that the effect of reactive elements can superpose this parameter.

Titanium (Ti) and zirconium (Zr) have an equivalent effect on the reduction of porosity. A large number of CuSn-, CuAlFe- and CuMnNi-alloy billets were spray formed with and without Ti. Density was measured by buoyancy balance. The data from these billets were used for calculating the mean porosity.

The comparison between calculated and analysed nitrogen and titanium-nitride concentration in the billet gives a clear indication of the mechanism of hot porosity formation. It is believed that the gas (nitrogen) is entrained by the droplets hitting the mushy layer on top of the substrate. This nitrogen reacts with titanium in the melt. Most of this occurs between liquidus and solidus temperature. Reaction below solidus temperature does not decrease porosity but can decrease gas pressure inside the pores. The calculations and measurements prove the theory of nitrogen filled pores and demonstrate how addition of Ti helps to reduce porosity.

## References

- [1] F. Akhlaghi, J. Beech, H. Jones: Influence of Operating Parameters on Characteristics of Aluminium Powders and Spray-Cast Deposits, Proceedings of the First International Conference on Spray Forming, 17th – 19th September 1990, Swansea, U.K.
- [2] G. Watson: Thermal and Microstructural Characterization of Spray Cast Copper Alloy Strip, Proceedings of the First International Conference on Spray Forming, 17th – 19th September 1990, Swansea, U.K.
- [3] L. Warner, C. Cai, S. Annavarapu, R. Doherty: Modelling Microstructural Development in Spray Forming: Experimental Verification, Proceedings of the Third International Conference on Spray Forming, 1996, Cardiff, U.K.
- [4] P.P. Maher, P.S. Grant, B. Cantor, L. Katgerman: Manufacture of Spray-Formed Al Based Alloys and Composites, Proceedings of the First International Conference on Spray Forming, 17th – 19th September 1990, Swansea, U.K.
- [5] R. Doherty, S. Annavarapu, C. Cai, L. K. Kohler: Modelling Based Studies for Control and Microstructure Development in Spray Forming, Kolloquiumsband Sprühkompaktieren, Universität Bremen, Band 2 (1997), 45 – 78
- [6] M. G. Chu: Microstructure of Aluminium Alloy Deposit Produced by Spray Forming Using a Linear Nozzle, Kolloquiumsband Sprühkompaktieren, Universität Bremen, Band 2 (1997), 115 – 130

- [7] M. Rein: Spray Deposition: The Importance of Droplet impact Phenomena, Kolloquiumsband Sprühkompaktieren, Universität Bremen, Band 3 (1998), 115 – 128
- [8] N. Jordan, H. Harig: Sprühkompaktierte Kupferbasis-Werkstoffe – Stand der Forschungs- und Entwicklungsarbeiten, Kolloquiumsband Sprühkompaktieren, Universität Bremen, Band 3 (1998), 31 – 52
- [9] W.G. Watson, S. Ashok, H.P. Cheskis: Method to Reduce Porosity in a Spray Cast Deposit, U.S. Patent Number 4 961 457, 9th Oct. 1990
- [10] R.H. Cooney, J.V. Wood: Production and Development of Copper-Base Alloys by the Osprey Process, Proceedings of the First International Conference on Spray Forming, 17th – 19th September 1990, Swansea, U.K.
- [11] E. Mathei-Schulz, A. Schulz, P. Mayer: Gefügeauswertung an sprühkompaktierten Werkstoffen mit bildanalytischen Methoden, Kolloquiumsband Sprühkompaktieren, Universität Bremen, Band 5 (2001), 179 – 191
- [12] H.R. Müller, S. Hansmann, K. Ohla: Influence of Process Parameters on Segregation and Porosity in Spray-Formed Cu-Sn-Billets, Spray Deposition and Melt Atomization Conference, 26. – 28. June 2000, Bremen, Germany, 205 – 218
- [13] M. Hedges: Spray Forming and Microstructure of Nickel Superalloys IN718 and RS5, D. Phil thesis, Oxford University, Dept. of Materials, 2003

- [14] J. Muller: XRD measurements on the ARL X'TRA diffractometer, Customer Result Report 0602, ARL Applied Research Laboratories S.A. En Vallaire Ouest C, CH-1024 Ecublens, Switzerland, 20.06.2002
- [15] M. Ebner: Nachweis von TiN-Phasen im sprühkompaktierten Material BC1, interner Laborbericht Nr. 1859 der Wieland-Werke AG, Ulm, 22.8.2002
- [16] A. Roine: Outokumpu HSC Chemistry for Windows, Chemical Reaction and Equilibrium Software with Extensive Thermochemical Database, User's guide Version 4.0 June 30 (1999), ISBN 952-9507-05-4

## Figure Captions

**Fig. 1: Classification of porosity in spray-formed deposits**

**Fig. 2: Microstructure and porosity of CuAl<sub>13</sub>Fe<sub>4.5</sub>CoMn,  $\rho_0 = 7.20 \text{ g/cm}^3$**

**Fig. 3: Microstructure and porosity of CuSn<sub>14.5</sub>,  $\rho_0 = 8.93 \text{ g/cm}^3$**

**Fig. 4: Microstructure and porosity of CuMn<sub>20</sub>Ni<sub>20</sub>,  $\rho_0 = 8.25 \text{ g/cm}^3$**

**Fig. 5: Overspray particle with embedded particle and two craters**

**Fig. 6: Density of CuAl<sub>13</sub>Fe<sub>4.5</sub>MnCo with and without Ti**

**Fig. 7: Density of CuSn<sub>13.5</sub>Pb with and without Ti**

**Fig. 8: Density of CuMn<sub>20</sub>Ni<sub>20</sub> with and without Ti**

**Fig. 9: Schematic diagram of the experimental set up for the electrolytic extraction of secondary phases**

**Fig. 10: Schematic diagram of the experimental set up for the filtration of extracted secondary phases from the electrolyte**

**Fig. 11: X-ray diffraction and theoretical diffraction diagram for TiN (Osbornite)**

**Fig. 12: Scheme of the mushy layer on top of the deposit with embedded gas bubbles**

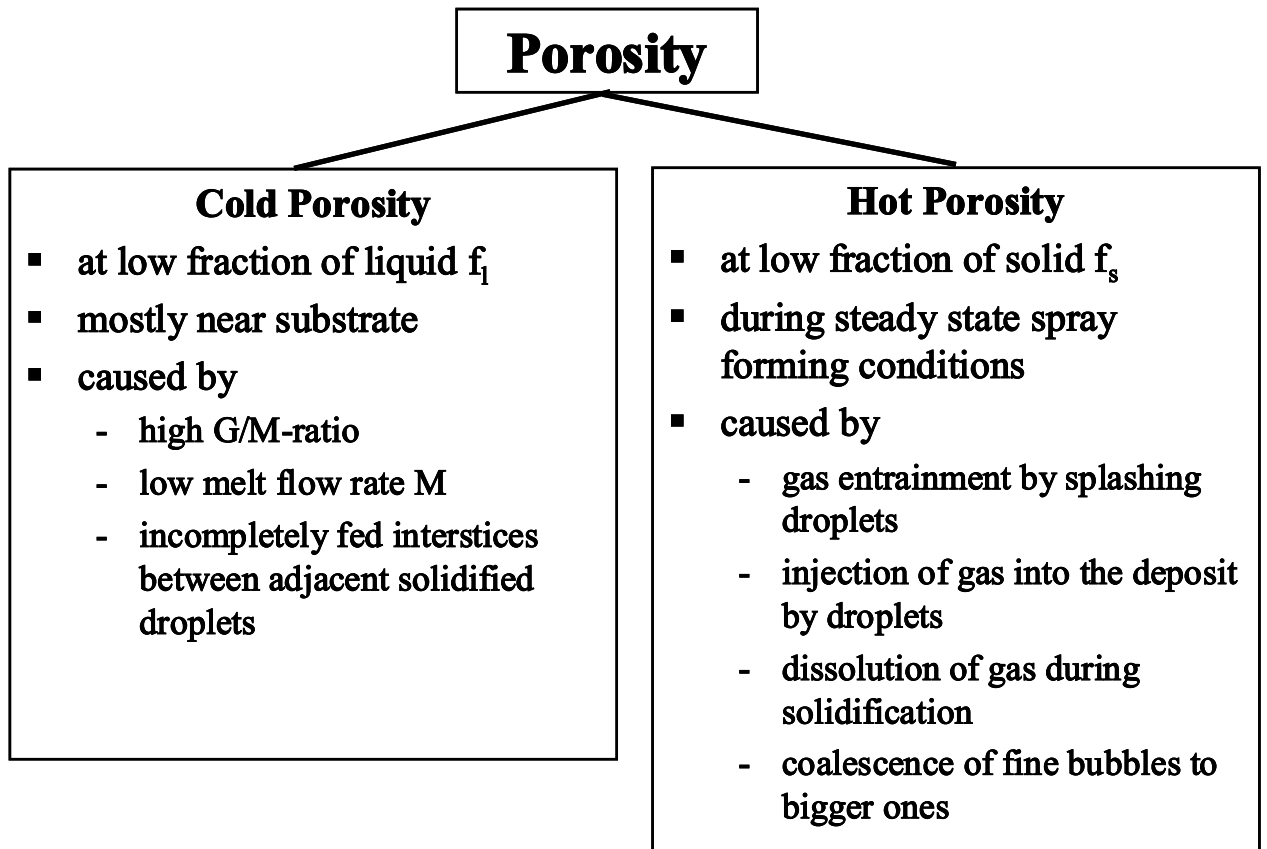
**Fig. 13: Mass of reaction products vs. temperature**

**Table 1:** Comparison of calculated with measured nitrogen concentration in the deposit

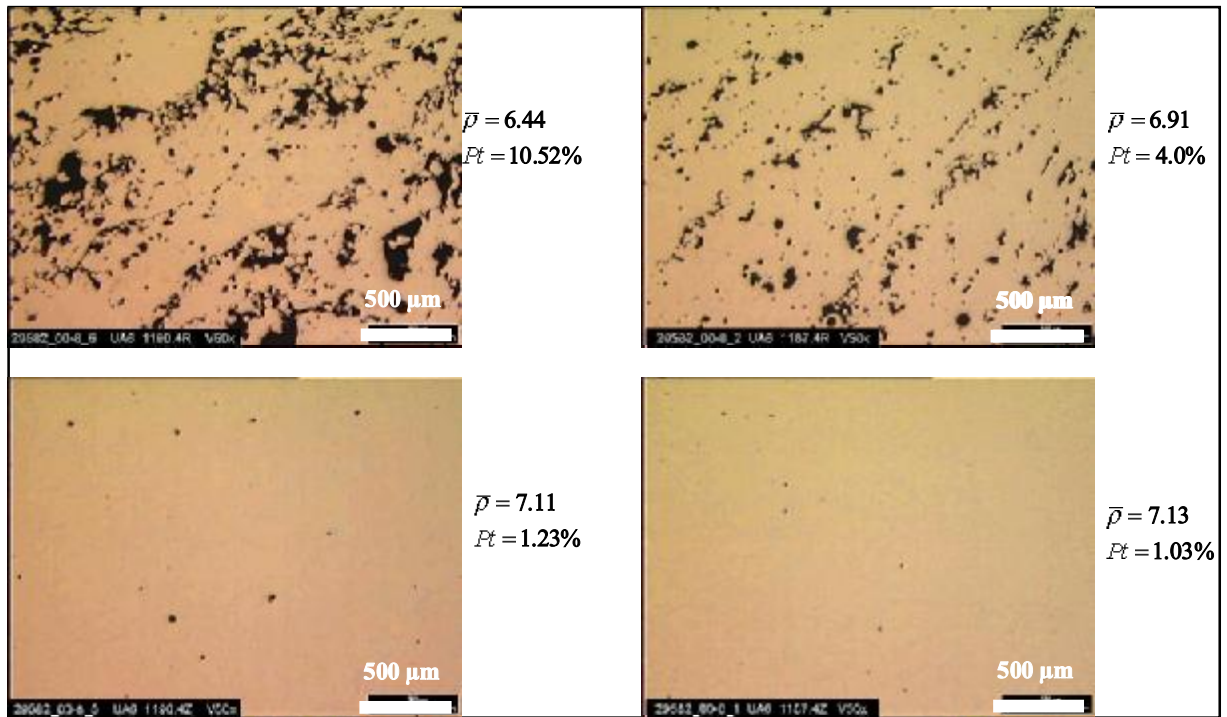
Alloy	Run	$\rho_0$	$\bar{\rho}_{\min}$	$\bar{\rho}_{\max}$	$Pt_{\min}$	$Pt_{\max}$	$c_{N_2,\min}$	$c_{N_2,\max}$	$c_{N_2,m}$
		g/cm <sup>3</sup>	g/cm <sup>3</sup>	g/cm <sup>3</sup>	%	%	%	%	%
CuSn13.5Pb	1528	8.95	8.60	8.71	2.68	3.91	0.00010	0.00015	0.00015
CuSn13.5	1736	8.93	8.65	8.81	1.34	3.14	0.00005	0.00012	0.00020

**Table 1:** Example calculation for CuMn20Ni20 with and without Ti

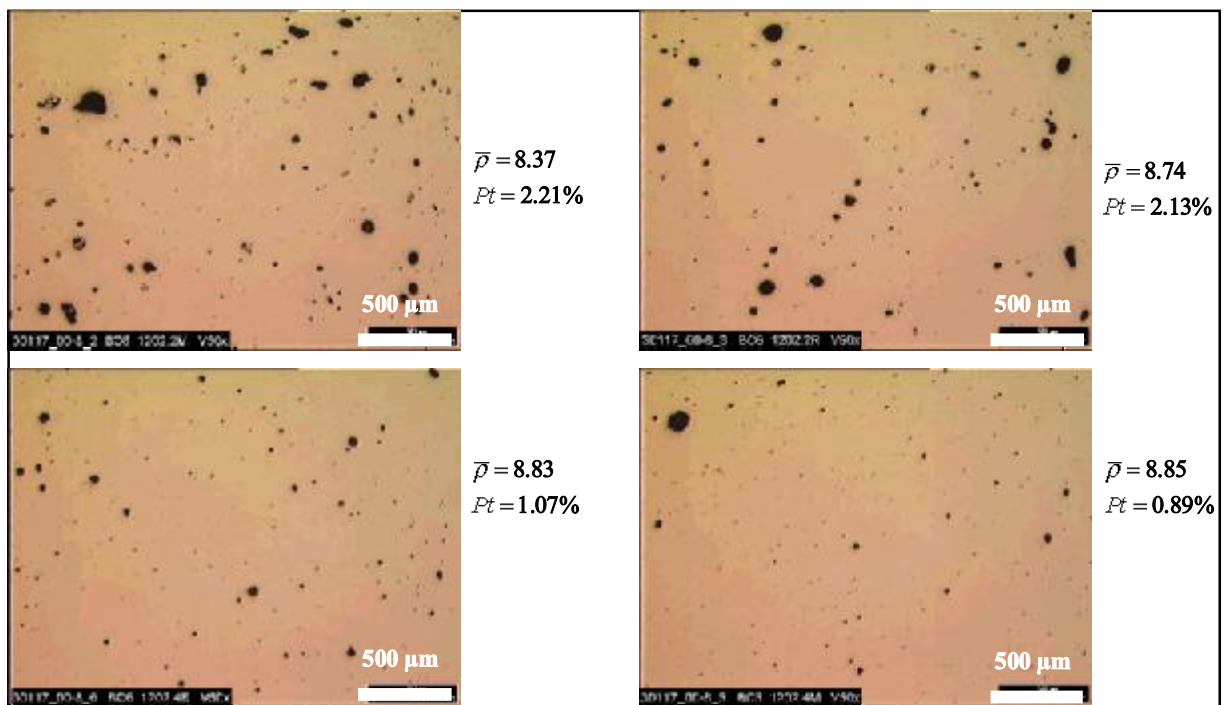
$\rho_0$	8.20 g/cm <sup>3</sup>	Density of pore free deposit
$\bar{\rho}$	8.05 g/cm <sup>3</sup>	Measured mean value of deposit without Ti
$\bar{\rho}_{Ti}$	8.15 g/cm <sup>3</sup>	Measured mean value of deposit with Ti
$m_D$	1500 kg	Mass of deposit
$\rho_N$	1.17 kg/m <sup>3</sup>	Density of gas at $\vartheta_N$ , 1 bar
$\vartheta_N$	15 °C	Standard temperature
$\vartheta_{sol}$	1005 °C	Solidus temperature
$\alpha$	1.86E-05 1/K	Thermal linear expansion coefficient
$\vartheta_a$	25 °C	Ambient temperature
$P_{liqu}$	0.1 MPa	Pressure at entrainment of bubble (chamber pressure)
$R$	8.31 J/mol K	Molar gas constant
$M_{Ti}$	47.90 g/mol	Molar mass of Ti
$M_N$	14.01 g/mol	Molar mass of N
$Pt$	1.83 %	Porosity without Ti
$Pt_{Ti}$	0.61 %	Porosity with Ti
$\rho_{sol}$	0.000264 g/cm <sup>3</sup>	Density of gas in pore at solidus temperature
$\rho_a$	0.000278 g/cm <sup>3</sup>	Density of gas in pore at ambient temperature
$V_D$	186,335.40 cm <sup>3</sup>	Volume of deposit without Ti
$V_{L,Ti}$	184,049.08 cm <sup>3</sup>	Volume of the deposit with Ti
$V_P$	3,409 cm <sup>3</sup>	Volume of the pores in the deposit without Ti
$V_{P,Ti}$	1,122 cm <sup>3</sup>	Volume of the pores in the deposit with Ti
$\Delta V$	2,286 cm <sup>3</sup>	Volume of N <sub>2</sub> reacted with Ti
$P_a$	0.0246 MPa	Pressure in pore at ambient temperature
$n$	0.023 mol	Number of moles N <sub>2</sub> reacted with Ti
$n_{Ti}$	0.045 mol	Number of moles Ti reacted with N
$m_{Ti}$	2.17 g	Mass of Ti reacted with N <sub>2</sub>
$c_{Ti}$	0.00014 %	Concentration of Ti needed for reaction
$n_N$	0.068 mol	Total number of moles N in pores of the deposit
$m_{N_2}$	0.948 g	Total mass N <sub>2</sub> in pores of the deposit
$c_{N_2}$	0.000063 %	Total concentration N <sub>2</sub> in the deposit
$m_{TiN}$	2.810 g	Mass of TiN in the deposit
$c_{TiN}$	0.00019 %	Concentration of TiN in the deposit



**Fig. 1:** Classification of porosity in spray-formed deposits

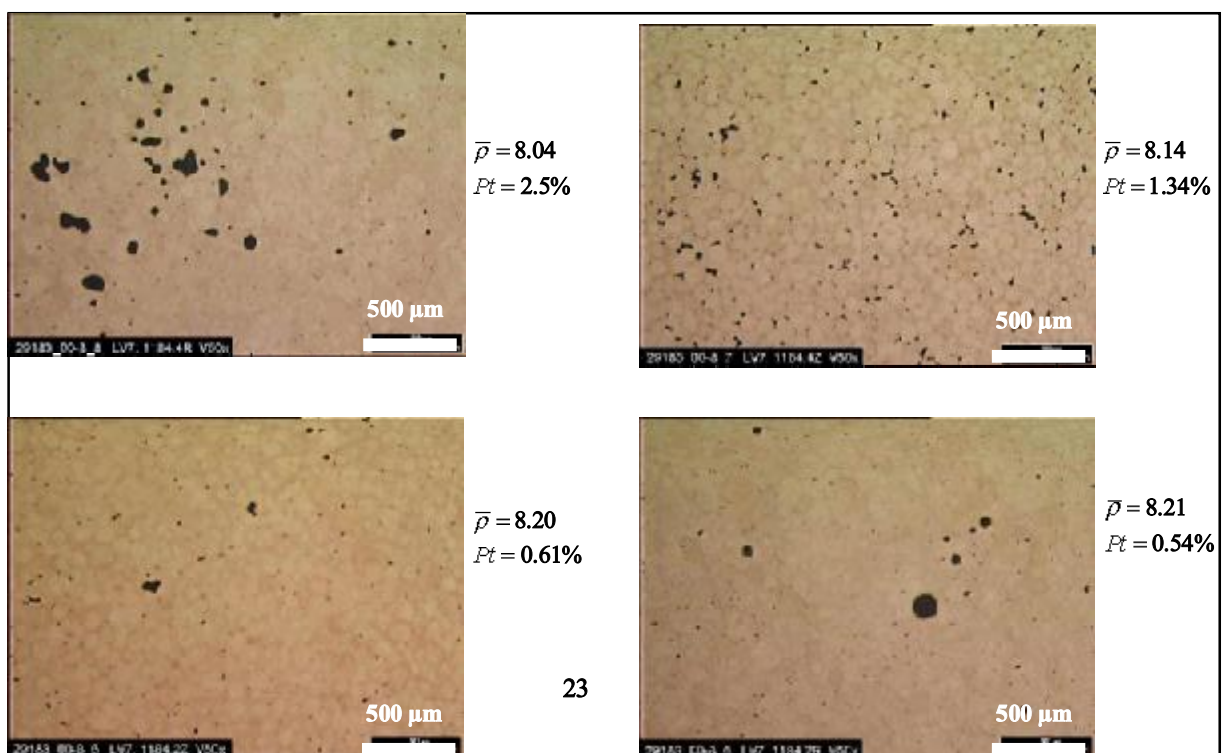


**Fig. 2:** Microstructure and porosity of CuAl13Fe4.5CoMn,  $\rho_0 = 7.20 \text{ g/cm}^3$



**Fig. 3:** Microstructure and porosity of CuSn14.5,  $\rho_0 = 8.93 \text{ g/cm}^3$

**Fig. 4:** Microstructure and porosity of CuMn20Ni20,  $\rho_0 = 8.25 \text{ g/cm}^3$



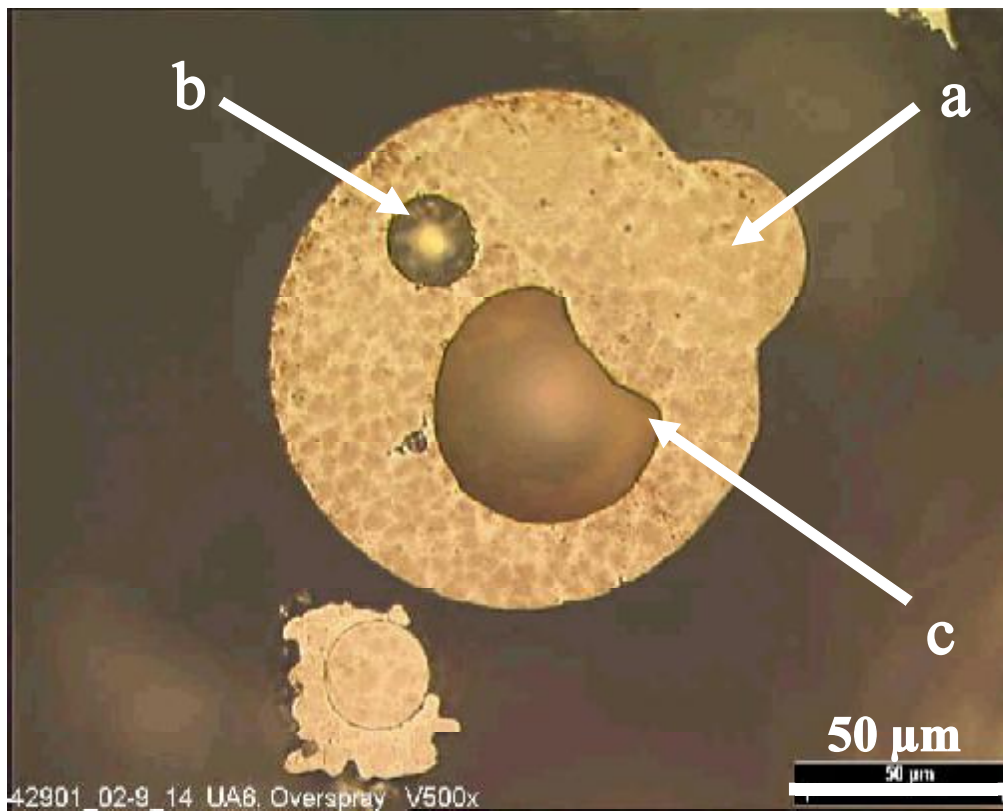


**Fig. 5:** Overspray particle with embedded particle and two craters

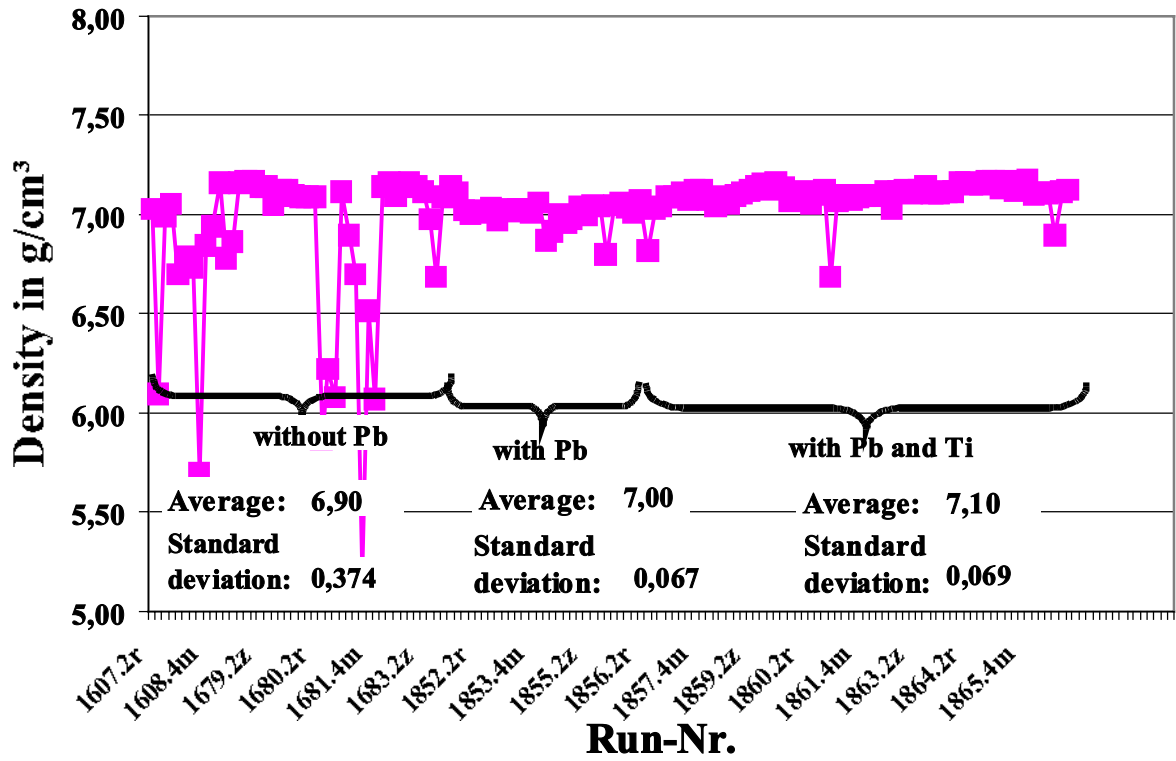


Fig. 6: Density of CuAl13Fe4.5MnCo with and without Ti

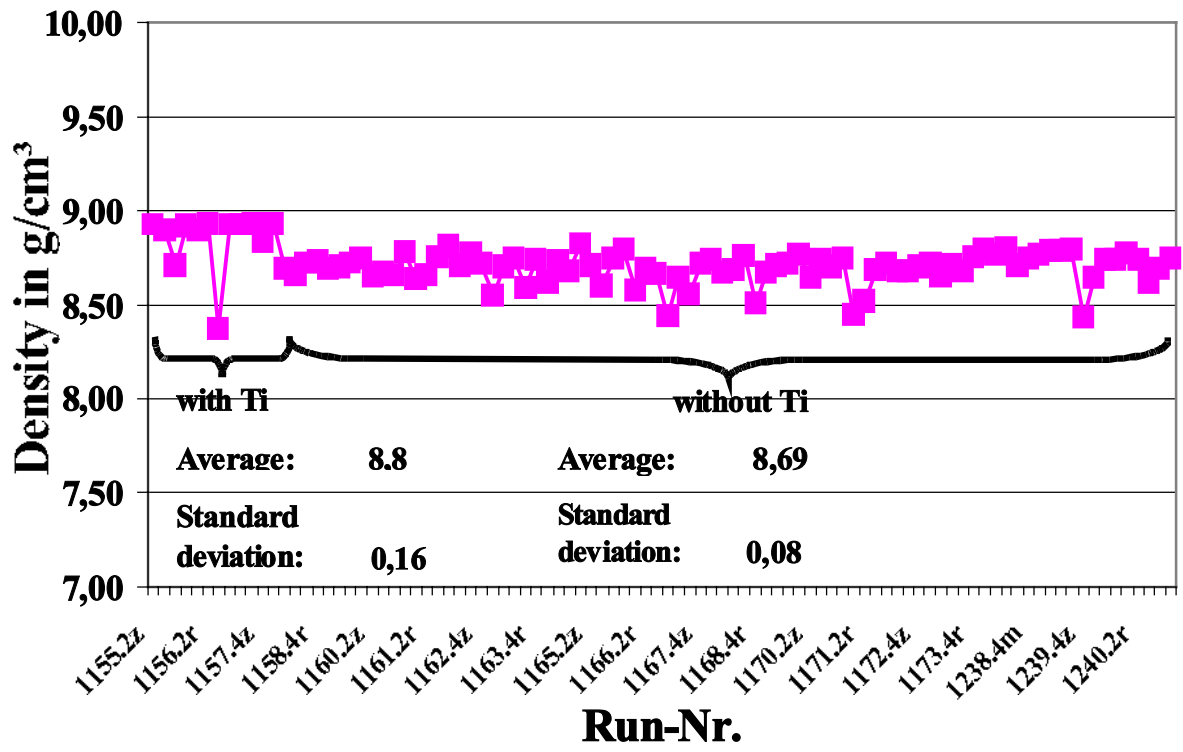


Fig. 7: Density of CuSn13.5Pb with and without Ti

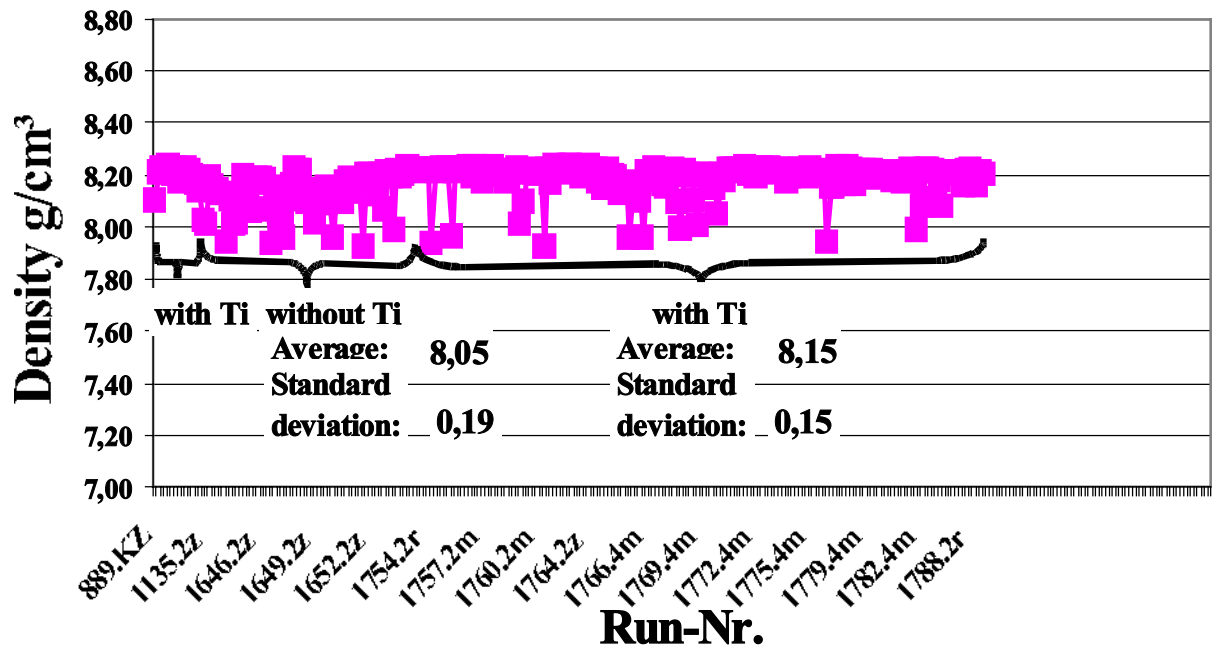
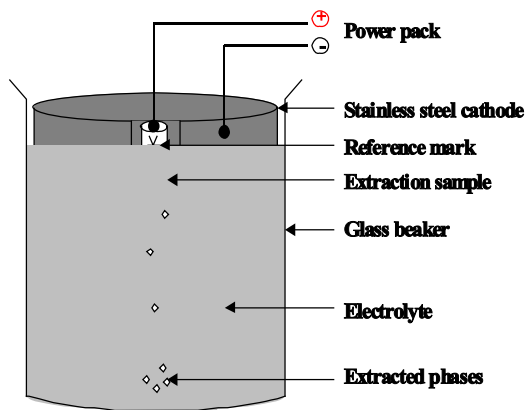
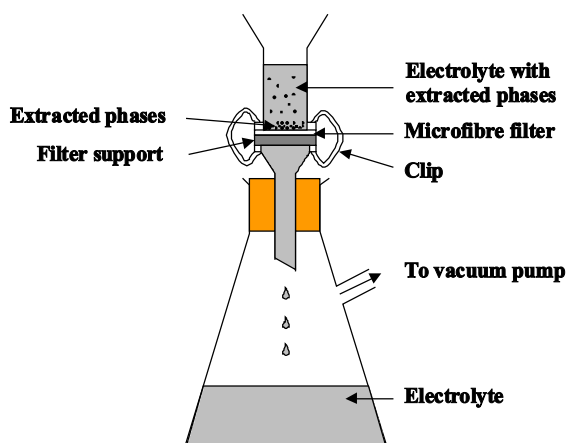


Fig. 8: Density of CuMn20Ni20 with and without Ti



**Fig. 9:** Schematic diagram of the experimental set up for the electrolytic extraction of secondary phases



**Fig. 10:** Schematic diagram of the experimental set up for the filtration of extracted secondary phases from the electrolyte

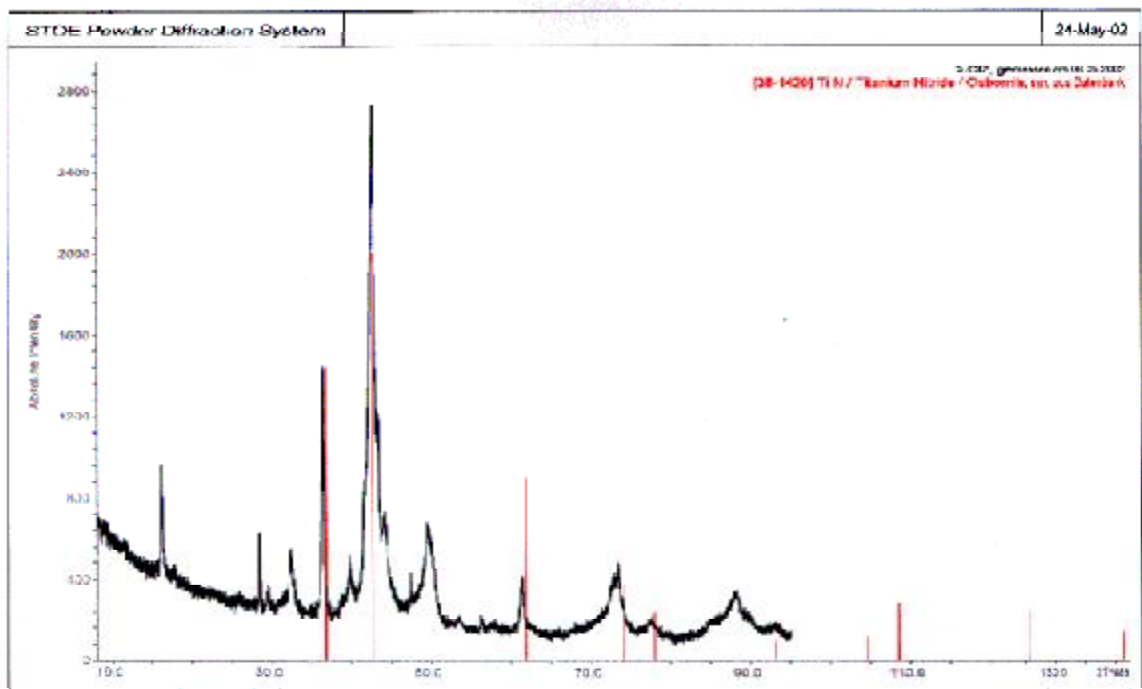


**Fig. 11:** X-ray diffraction and theoretical diffraction diagram for TiN (Osbornite)

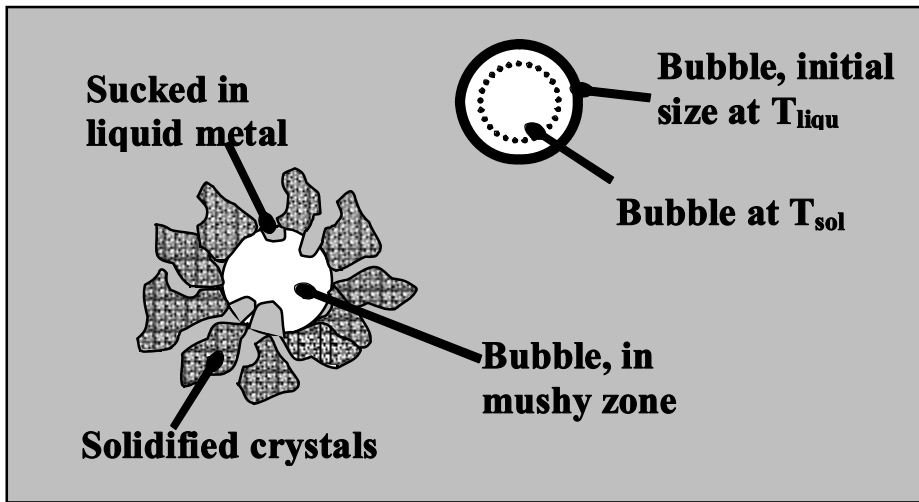


**Fig. 12:** Scheme of the mushy layer on top of the deposit with embedded gas bubbles

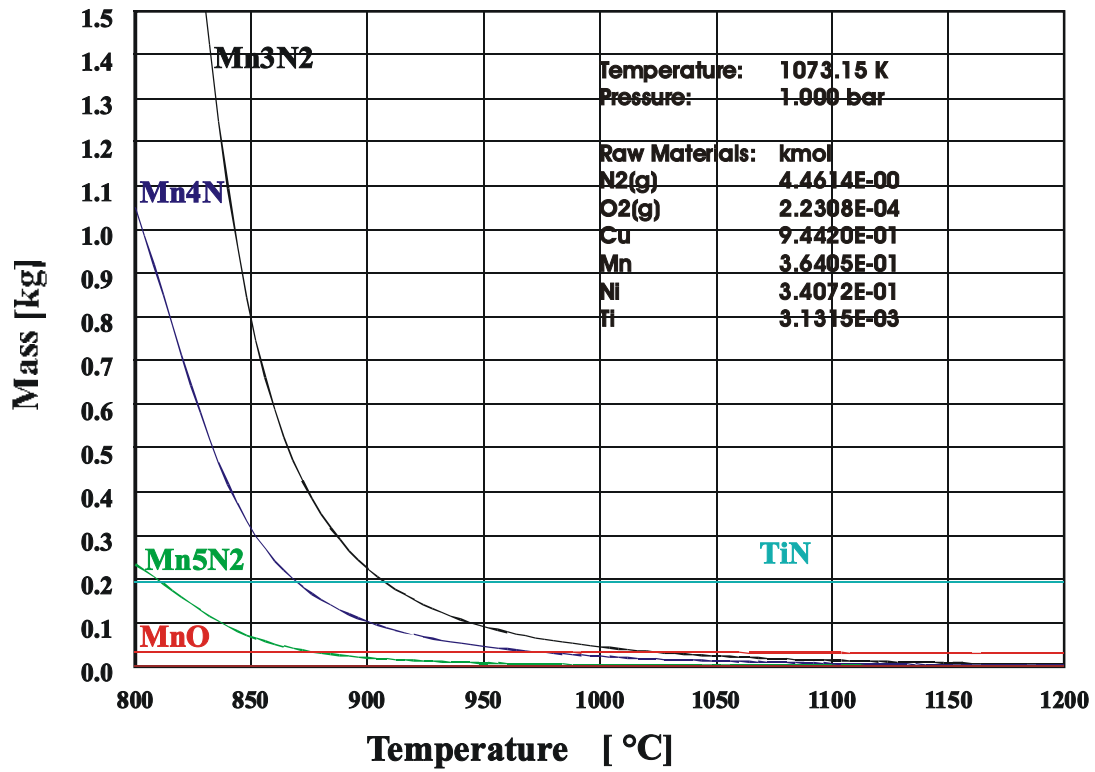


Fig. 13: Mass of reaction products vs. temperature